JOURNAL OF GEOPHYSICAL RESEARCH, VOL. 94, NO. B7, PAGES 9439-9451, JULY 10, 1989

The Influence of Groundwater Flow on Thermal Regimes in Mountainous Terrain: A Model Study

CRAIG FORSTER

Department of Geology, Utah State University, Logan

LESLIE SMITH

Department of Geological Sciences, University of British Columbia, Vancouver

Groundwater flow in high-relief mountainous terrain is modeled to examine how geology, surface topography, climate, and regional heat flow influence the pattern and magnitude of an advective thermal disturbance. A numerical procedure is used to estimate the position of the water table within constraints provided by the available infiltration rate and the permeability of the mountain massif. Results show that where the water table is located at depth within the mountain massif, the rate of groundwater recharge, rather than permeability, is the appropriate factor to characterize the potential for an advective disturbance. Thermal disturbances should be assessed within the framework of the two-dimensional character of the flow system because interpretations based on one-dimensional models are prone to significant error. Modeling of site-specific systems can exploit the existence of a permeability "window," where temperatures in discharge areas and in springs discharging from fracture zones reach peak values. Temperatures of thermal springs reflect the complex interaction between flow within the mountain massif and flow through permeable fracture zones. Consequently, simple calculations relating the geothermal gradient, depth of maximum groundwater circulation, and discharge temperature improperly represent the physics of the process.

INTRODUCTION

Ongoing interest in characterizing the Earth's thermal state, investigating the nature of certain geologic processes within the upper crust, and exploring for geothermal resources has led to the collection of heat flow data in mountainous regions. A subset of these data indicates that groundwater flow can cause a significant advective disturbance of thermal regimes [*Steele and Blackwell*, 1982; *Mase et al.*, 1982; *Black et al.*, 1983; *Reader and Fairbank*, 1983]. Although advective disturbance of thermal regimes has long been recognized (see review by *Lachenbruch and Sass* [1977]), the interaction of groundwater flow and heat transfer within a mountain massif has received little study.

Schematic flow systems shown in Figure 1 illustrate the amplitude and wavelength of groundwater flow systems that might develop in both high-relief and low-relief terrain. Greater relief found in mountainous terrain causes an enhanced vertical component of groundwater flow that, in turn, may enhance advective disturbance of the thermal regime. Furthermore, closely spaced ridges and valleys in high-relief terrain cause an advective disturbance that has a restricted lateral extent when compared to the long-wavelength disturbances typical of low-relief terrain. As a consequence, groundwater flow within a mountain massif can cause large-amplitude, short-wavelength perturbations of the thermal regime that may distort our view of broad regional-scale variations in heat flow. With few exceptions [*Steele and Blackwell*, 1982; *Reader and Fairbank*, 1983], most thermal data sets in mountainous terrain are obtained from isolated boreholes located at the valley floor or at lower elevations on the mountain flank. In addition, distances separating boreholes often exceed 5 km. Inferences based on these sparse and selectively distributed data may provide little insight into regional heat flow in mountainous terrain. In contrast, groundwater flow systems in low-relief terrain can cause perturbations that are relatively easy to characterize using heat flow data collected from boreholes separated by distances exceeding several tens of kilometers [*Willet and Chapman*, 1987]. Such data sets have helped constrain model studies that illustrate how basin-scale thermal regimes in low-relief terrain can be perturbed by regional groundwater flow [*Brott et al.*, 1981; *Smith and Chapman*, 1983; *Garven and Freeze*, 1984; *Woodbury and Smith*, 1985; *Gosnold*, 1985; *Majorowicz et al.*, 1985).

Numerical models provide a quantitative framework for interpreting subsurface temperature data collected in mountainous terrain. *Hanoaka* [1980] examines the influence of surface topography on the interaction between topographically driven fluid flow and free convection by modeling idealized, steady state hydrothermal systems. While a nonuniform distribution of regional heat flow is implicitly specified; *Hanoaka* [1980] did not address the issues of climate, different conditions of regional heat flow, and depth to the water table. *Ingebritsen and Sorey* [1985] incorporated the influence of high-relief topography in their transient numerical model of advection-dominated heat transfer at Mount Lassen, Oregon. Because a basal source of heated fluid is used to represent the circulation and heating of groundwater recharged on the mountain flanks, the relationship between the magnitude of the fluid source and rates of groundwater recharge at the ground surface is poorly defined. Recent hydrologic modeling performed by *Forster and Smith*, 1988*b* illustrates patterns of groundwater flow expected within a mountain massif under a variety of geologic, climatic, and topographic conditions.

Our approach differs from those of *Hanoaka* [1980] and *Ingebritsen and Sorey* [1985] in two key respects. First, we explore the influence of climate on advective heat transfer by specifying recharge to the flow system as an input variable

Paper number 89JB00297.
0148-0027/89/89JB-00297$05.00

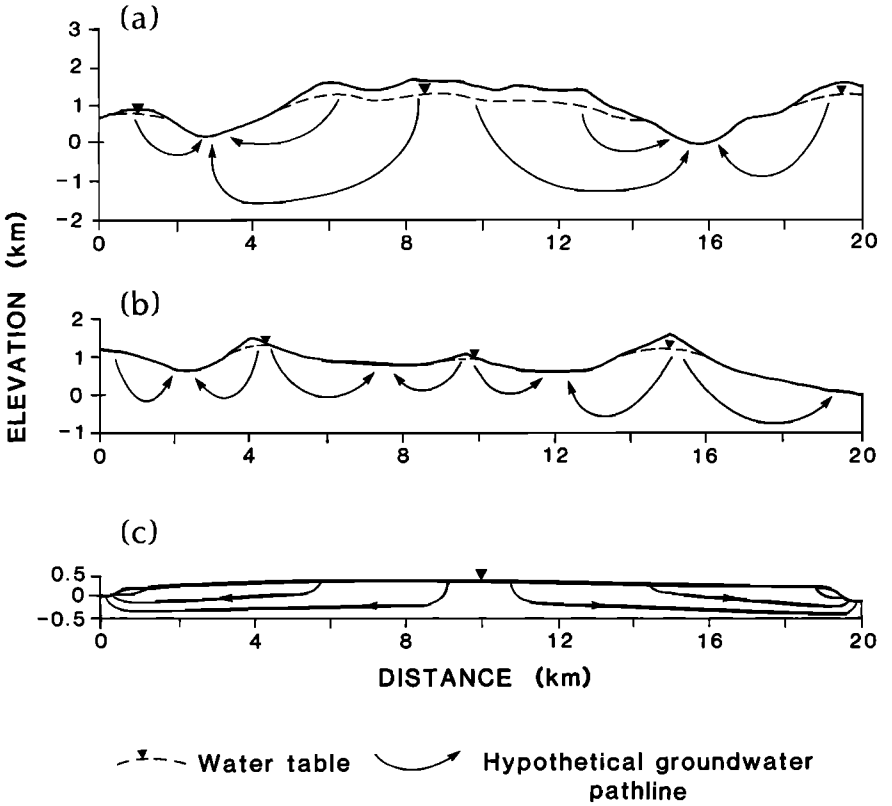

Fig. 1. Schematic groundwater flow systems for (*a*) Coast Mountains of British Columbia, (*b*) Rocky Mountains of British Columbia-Alberta, and (*c*) conventional low-relief terrain after *Freeze and Witherspoon* [1967].

rather than assuming an arbitrary water table configuration. This is accomplished using a free-surface modeling technique. Second, we incorporate permeable fracture zones as discrete entities that play an important role in the development of thermal springs. This approach has enabled us to characterize the nature of groundwater flow systems in mountainous terrain and to demonstrate the important influence of the thermal regime on mountain-scale flow systems [*Forster and Smith*, 1988*b*]. This paper expands our work to examine the influence of fluid flow on thermal regimes. The modeling results have implications for assessing the way that advective heat transfer modifies the near-surface expression of regional heat flow, controls the genesis of landform-controlled ore deposits, and influences the development of geothermal systems. Topics to be considered include (1) the nature and magnitude of advective heat transfer, (2) the interaction of thermally driven free convection and topographically driven forced convection within a mountain massif, (3) the transfer of heat within fracture zones, and (4) the nature of thermal springs. Following the example of *Thompson* [1964], mountainous terrain is defined as rugged topography with local relief in excess of 600 m.

APPROACH

Our conceptual model for groundwater flow and heat transfer is shown in Figure 2. Vertical boundaries are insulated and impermeable, reflecting a periodic repetition in surface topography with wavelength of 12 km and amplitude of 2 km. This topography resembles conditions found in the Coast Mountains of British Columbia (Figure 1*a*), the Rocky Mountains of Canada and the United States (Figure 1*b*), and the central Cascades of the Pacific Northwest. The horizontal basal boundary is assumed impervious to fluid flow. Regional conductive heat flow is represented by a uniform heat flux (H_b) applied across the basal boundary.

The upper boundary of the domain is the bedrock surface. The thin cover of discontinuous surficial deposits typical of upland areas of mountain slopes is viewed as a thin skin of variable thickness that is not explicitly included in the model. Resistance to heat transfer in the thin surficial deposits is assumed negligible so temperatures at the bedrock surface match those at the ground surface. Surface temperature conditions are defined in terms of a reference surface temperature (T_r) and a thermal lapse rate (G_l). Exceptions occur where fractures outcrop to produce springs. In such cases, temperatures at the bedrock surface are assumed to reflect the temperature of groundwater flowing in the fracture zone rather than the ambient air temperature.

In earlier numerical studies of coupled fluid flow and heat transfer in regional-scale flow systems, it is assumed that the water table is the upper boundary of the flow domain [e.g., *Smith and Chapman*, 1985]. An important limitation of this approach is that the magnitude and spatial distribution of groundwater recharge are imposed implicitly when a water table configuration is specified explicitly. Modeling results indicate that it is preferable to estimate the water table position within the constraints of groundwater recharge rate, basal heat flow, and permeability [*Forster and Smith*, 1988*b*]. If this alternative approach is not adopted, varying values of permeability or heat flow in a sensitivity analysis may yield unrealistic values for groundwater recharge. These results

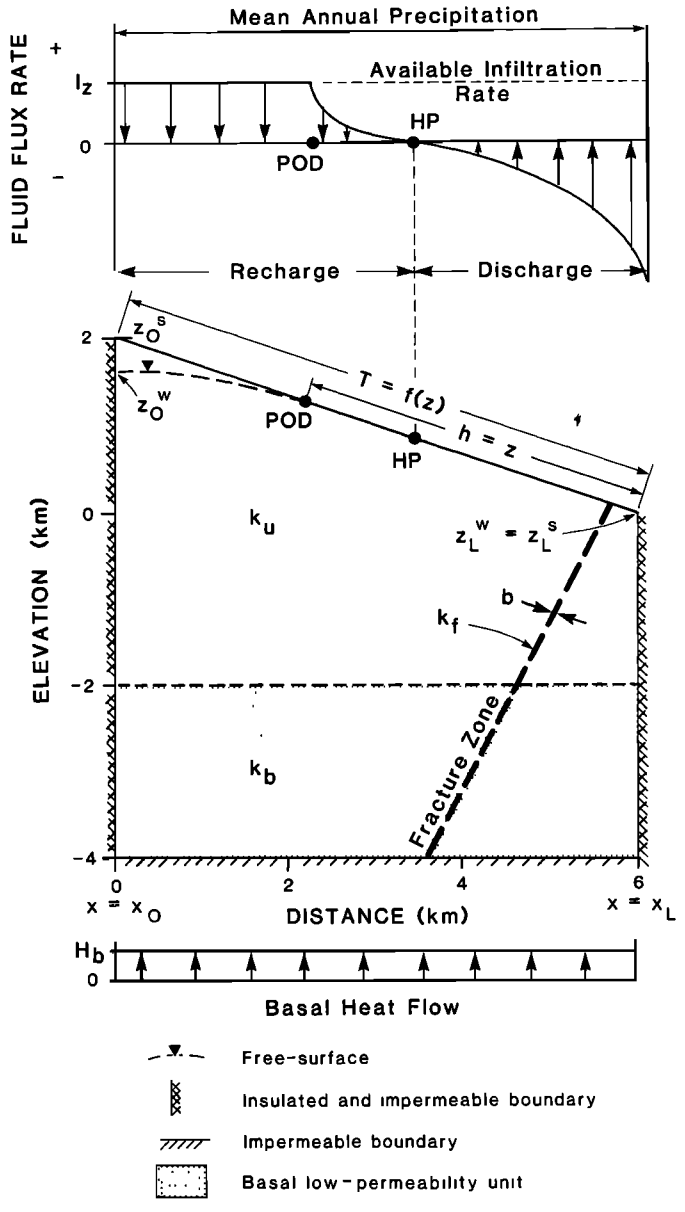

Fig. 2. Conceptual model for groundwater flow and heat transfer in mountainous terrain. POD (point of detachment) and HP (hinge point) are terms defined to describe the points where the water table intersects the ground surface and the transition between recharge and discharge, respectively. Z_0^w and Z_L^w define the elevation of the water table at X_0 and X_L. Z_0^s and Z_L^s define the elevation of the ground surface at X_0 and X_L. A more detailed description of the boundary value problem is given by *Forster and Smith*, 1988*a*.

can, in turn, have an important impact on the pattern and magnitude of advective heat transfer. Therefore, when simulating large ranges in the values of permeability and heat flow, it is important to explicitly constrain fluid flux across the upper boundary. This constraint can be imposed by assuming that the water table need not coincide with the upper boundary, which in our study is assumed to be the bedrock surface.

Fluid moving within the thin skin of surficial deposits is lumped with overland flow as a runoff term. The remaining fluid available for recharge, termed an available infiltration rate I_z, is the vertical volumetric flux of fluid across a horizontal plane of unit area ($(m^3\ s^{-1})\ m^{-2}$). In the absence of detailed field data, I_z is best thought of as a percentage of the mean annual precipitation rate (Figure 2). By providing explicit control on groundwater recharge, this modeling approach allows us to examine the influence of various climatic environments (e.g., ranging from arid to humid) on the nature and magnitude of fluid flux and advective heat transfer.

The available infiltration rate represents an upper limit for recharge to the groundwater flow system. Where the water table coincides with the bedrock surface, only a portion of the available infiltration is transmitted to the bedrock. The remainder is contributed to surface runoff. The ability of the flow system to transmit the incoming fluid depends upon a variety of factors including topographic relief, rock permeability, and basal heat flow [*Forster and Smith*, 1988*b*]. Where the water table lies below the bedrock surface, the entire available infiltration rate is assumed to cross the bedrock surface to be transmitted directly to the water table via one-dimensional flow through an unsaturated zone. Adopting this approach enables us to control the pattern and magnitude of groundwater recharge without specifying, a priori, the position of the water table.

Heat is transferred by both conduction and advection throughout the domain shown in Figure 2. Advective heat transfer above the water table is represented by one-dimensional movement of fluid, in the liquid phase, at a rate determined by the available infiltration rate. By assuming that the lower limit for infiltration rate is 10^{-12} m s^{-1}, vapor movement can be taken to be negligible [*Ross*, 1984]. Unsaturated zones with infiltration rates less than this amount are likely found only in the most arid of climates. A reasonable upper limit for available infiltration rates is about 2×10^{-8} m s^{-1} or 0.6 m yr^{-1} [*Forster and Smith*, 1988*b*].

A basal low-permeability unit occupies the lower 2 km of the domain to provide a region of conduction-dominated heat transfer (Figure 2). The remainder of the domain contains a higher-permeability unit where advective heat transfer may dominate. Although values of bulk permeability are likely controlled by the degree of fracturing within the rock mass, we treat the rock mass as an equivalent porous medium. Exceptions to this assumption are represented as discrete permeable fracture zones with a homogeneous permeability k_f and width b (Figure 2).

The mathematical model describing the system shown in Figure 2 is expressed by coupled partial differential equations for heat transfer and fluid flow, by equations of state for the fluid properties, and by boundary conditions for the thermal and fluid flow problems. Readers interested in details of the mathematical model are referred to *Forster and Smith* [1988*a*]. Key assumptions include (1) steady state fluid flow and heat transfer in a saturated porous medium with one-dimensional fluid flow through the unsaturated zone at the available infiltration rate, (2) no internal heat sources or sinks, (3) thermal springs presumed to discharge only from major through-going fractures intersecting the bedrock surface, (4) thermal equilibrium existing between fluid and solid, (5) the fluid being pure liquid water with density and viscosity a function only of temperature and pressure, (6) the heat capacity and thermal conductivity of the fluid being constant, and (7) porosity, permeability, and thermal conductivity

TABLE 1. TYPICAL SIMULATION PARAMETERS

Parameter	Definition	Value
	Fluid Flow Parameters	
k_b	permeability of basal unit	1.0×10^{-22} m^2
k_u *	permeability of upper unit	1.0×10^{-15} m^2
I_z *	vertical infiltration rate	2.0×10^{-9} m s^{-1}
	Thermal Parameters	
H_b *	basal heat flow	60.0 mW m^{-2}
G_l	surface temperature gradient	5 °C km^{-1}
T_r	reference surface temperature	10°C
n_b	porosity of basal unit	0.01
n_u	porosity of upper unit	0.10
λ^s	solid thermal conductivity	2.50 W m^{-1} °K^{-1}
λ^f	fluid thermal conductivity	0.58 W m^{-1} °K^{-1}
λ^v	vapor thermal conductivity	0.024 W m^{-1} °K^{-1}
C_f	specific heat capacity of water	4186.0 J kg^{-1} °C^{-1}
S	saturation above water table	0.0
α_l	longitudinal thermal dispersivity	100.0 m
α_t	transverse thermal dispersivity	10.0 m

* Parameters varied in the simulation series.

varying in space but not as a function of temperature or pressure.

In adopting this approach, we neglect a variety of factors (slope aspect, transients in surface temperature and groundwater flow, and complex heterogeneities in thermal and hydraulic properties) in order to concentrate on the character of advective heat transfer within a mountain massif. The influence of these factors on groundwater flow systems and hence on advective heat transfer has been assessed by *Forster and Smith* [1988*b*]. Factors other than long-term hydrologic and thermal transients caused by climate changes or igneous activity are judged to be of secondary importance [*Forster and Smith*, 1988*b*]. We are in the process of modifying the model to accommodate thermal transients caused by igneous activity. The equations describing fluid flow and heat transfer are solved using a Galerkin finite element technique. The water table elevation is estimated using an iterative free-surface method that is constrained by the available infiltration rate applied at the bedrock surface. Two-dimensional vertical sections with planar or radial symmetry are represented by linear triangular elements. Thin, high-permeability fracture zones are included by embedding one-dimensional line elements in the field of triangular elements. Details of the computational procedure are given by *Forster and Smith* [1988*a*].

RESULTS OF NUMERICAL SIMULATIONS

Simulations are performed by assigning a set of fluid flow and thermal parameters (Table 1) within a geometry similar to that of Figure 2. Characteristic variations in surface topography are incorporated by considering two extremes in slope profile (Figure 3): a convex topographic profile typical of glaciated crystalline terrain and a concave profile common in volcanic terrain. In most simulations, both upper and lower zones have homogeneous and isotropic permeability (k_u, k_b) and uniform porosity (n_u, n_b). More complicated variations in permeability and porosity (e.g., decreasing k and n with increasing depth) have been simulated with the model; however, the overall character of the results differs little from that obtained with the two homogeneous units. Although rock thermal conductivity (λ^s) is uniform throughout the system, varying porosity and saturation produce contrasts in effective thermal conductivity (λ^e). Longitudinal and transverse thermal dispersivities (α_l, α_t) are uniform and are held constant for all simulations.

In the following paragraphs, frequent reference is made to a reference case simulated using the parameter values listed in Table 1. Results for the reference case, shown in Figure 3*c*, are used as a standard for comparison with subsequent simulation results. The reference I_z of 2×10^{-9} m s^{-1} represents the rate of infiltration that might reasonably be available for recharge in a climate transitional between semiarid and humid. The upper unit permeability (k_u) of 10^{-15} m^2 represents relatively permeable conditions typical of moderately fractured crystalline or argillaceous rock [*Freeze and Cherry*, 1979; *Neuzil*, 1986]. The reference heat flux (H_b) of 60 mW m^{-2} is a typical conductive regional heat flux. Thermal conductivity (λ^s) is uniformly fixed at 2.5 W m^{-1} °K^{-1} (typical of values reported for crystalline rocks). *Barry* [1981] suggests that atmospheric thermal lapse rates may vary from less than 2 °C km^{-1} to greater than 8 °C km^{-1}. In this study, temperatures at the bedrock surface are defined using a median lapse rate (G_l) of 5 °C km^{-1} and a valley reference temperature (T_r) of 10°C.

Patterns of Advective Heat Transfer

Patterns of groundwater flow are depicted in Figure 3 by path lines (dotted lines) representing the track of a fluid particle entering the flow system at a specified point on the bedrock surface. Path line spacing is inversely proportional to the flux of fluid (specific discharge) through flow tubes

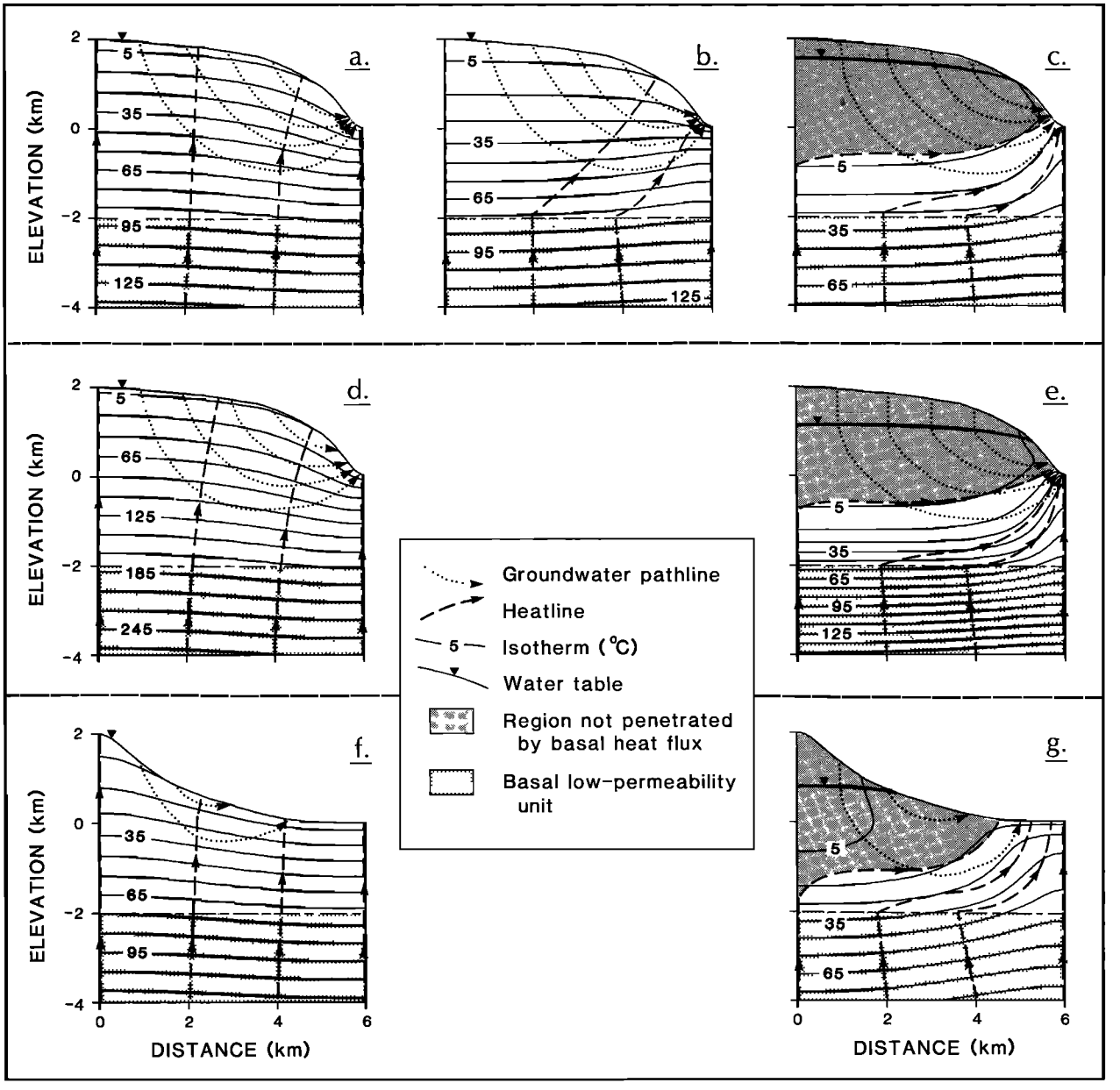

Fig. 3. Patterns of groundwater flow and heat transfer in convex and concave topography simulated with the reference conditions of Table 1 (except where noted); (*a*) $k_u = 10^{-18}$ m^2, (*b*) $k_u = 10^{-16}$ m^2, (*c*) $k_u = 10^{-15}$ m^2 (reference case), (*d*) $k_u = 10^{-18}$ m^2 and $H_b = 120$ mW m^{-2}, (*e*) $k_u = 10^{-15}$ m^2 and $H_b = 120$ mW m^{-2}, (*f*) $k_u = 10^{-18}$ m^2, (*g*) $k_u = 10^{-15}$ m^2.

bounded by each pair of pathlines. For example, path line spacing in the reference case (Figure 3*c*) varies because fluid flux in the convex domain increases approximately fivefold from a value of 2×10^{-9} m s^{-1} at the free surface to about 10^{-8} m s^{-1} at the discharge area. Fluid flux is more uniform in the concave domain (Figure 3*g*), decreasing from 2×10^{-9} m s^{-1} at the free surface to about 1.6×10^{-9} m s^{-1} at the discharge area.

Although similar, path lines that are defined by tracking the trajectories of fluid particles should not be confused with streamlines. These approaches differ because flow of fluid through each stream tube (bounded by each pair of streamlines) is fixed throughout the domain, while fluid flow through flow tubes defined on the basis of path lines may differ from flow tube to flow tube. Flow tubes shown in Figure 3 carry the same total flow only when the flow tubes intersect the free surface with equal spacing (recall that a uniform fluid flux is explicitly applied at the free surface).

Patterns of heat transfer are shown in Figure 3 by heat lines (thick dashed lines), while subsurface temperatures are represented by isotherms (solid lines). *Kimura and Béjan* [1983] suggest that heat lines are useful for mapping the transfer of thermal energy by conduction and advection. By definition, any heat line is locally parallel to the direction of net energy flow through the domain. Note that this yields heat lines normal to the isotherms only in regions where advective heat transfer by groundwater flow is negligible or where the direction of fluid flow is normal to the isotherms. Heat lines are everywhere normal to isotherms in the conduction-dominated thermal regimes shown in Figures 3*a*, 3*d*, and 3*f*. In this study, heat lines are identified by tracking

the advective and conductive transport of thermal energy originating at the basal boundary. Because a uniform heat flow is applied at the basal boundary, each heat tube (bounded by two heat lines) carries the same total thermal energy.

Heat lines and isotherms shown in Figure 3 illustrate the increasing influence of advective heat transfer as rock permeability is increased by three orders of magnitude. In each case, the available infiltration rate is fixed at the reference value (I_z = 2 x 10^{-9} m s^{-1}). Three series of simulation results are shown; the convex domain with reference heat flow (Figures 3*a*-3*c*), the convex domain with doubled heat flow (Figures 3*d* and 3*e*) and the concave domain with reference heat flow (Figures 3*f* and 3*g*). Conductive temperature fields, obtained for k_u equal to 10^{-18} m^2, are shown in the left-hand panel of each series (Figures 3*a*, 3*d*, and 3*f*). An advective disturbance, characterized by heat lines at an oblique angle to the isotherms, is evident when k_u exceeds about 10^{-16} m^2 (Figure 3*b*). A strong disturbance, shown in the right-hand panel of each series, is identified by heat lines subparallel to isotherms when k_u exceeds about 10^{-15} m^2 (Figures 3*d*, 3*e*, and 3*g*). *Woodbury and Smith* [1988] use the dependence of the thermal regime on bulk permeability in developing an inverse approach for estimating the bulk permeability of a mountain massif.

Temperatures within the shaded areas shown in Figures 3*c*, 3*e*, and 3*g* reflect the temperature of groundwater recharge at the bedrock surface because the basal heat flow is effectively masked by downward flowing groundwater. Elsewhere, heat line patterns indicate that the entire basal heat flow is absorbed by the circulating groundwater and redirected to exit in the discharge area.

Changes in permeability or basal heat flow are accompanied by little change in patterns of groundwater flow (Figure 3). Because rates of fluid flow increase as k_u or H_b is increased, reduced water table elevations are found in higher-permeability or higher heat flow cases (Figures 3*c*, 3*e*, and 3*g*). A reduced thermal disturbance is found for the concave slope profile (compare Figure 3*c* to Figure 3*g*) because smaller volumes of groundwater are transmitted at slower rates through the concave domain [*Forster and Smith*, 1988*b*].

In systems with a deep water table (greater than 50 m deep), permeability is not the factor that best characterizes the potential for a thermal disturbance. Rather, the rate of groundwater recharge best characterizes the rate of fluid flux through the domain. For example, reducing the value of I_z by a factor of 5, from 2 x 10^{-9} to 4 x 10^{-10} m s^{-1} (reflecting a transition to a more arid climate than that of Figure 3*c*), causes a fivefold decrease in groundwater flux and a significant decline in water table elevation (Figure 4). Reduced fluid flux creates a weaker thermal disturbance and a warmer thermal regime than that found for the higher-infiltration case of Figure 3*c*. This result could not be predicted on the basis of permeability alone because the rate of fluid flux is controlled by the infiltration rate. Furthermore, implicit infiltration rates resulting from arbitrary estimates of water table configurations may be inconsistent with the presumed conditions of climate and permeability. Adopting the free-surface approach reduces the dependence of model results on the difficult-to-estimate water table position and provides an additional constraint on the results by providing explicit control of estimated infiltration rates [*Forster and Smith*, 1988*b*].

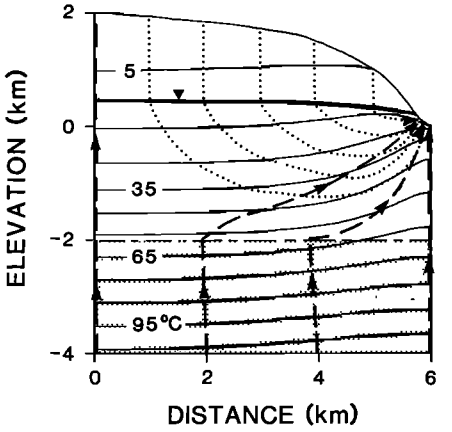

Fig. 4. Patterns of groundwater flow and heat transfer when I_z is reduced fivefold from that of the reference case (Figure 3*c*) to 4 x 10^{-10} m s^{-1}.

Magnitude of Advective Thermal Disturbance

The magnitude of an advective thermal disturbance can be characterized by noting the magnitude and spatial variation of two effects: (1) the degree that conductive thermal regimes are cooled, or heated, by groundwater circulation, and (2) the impact of advective heat transfer on vertical temperature gradients. These effects are illustrated in contour plots of temperature residuals and temperature gradient ratios (Figure 5). Temperature residuals are calculated by subtracting temperatures obtained for a given simulation from those of the corresponding conductive case, at each node in the finite element mesh. Figures 5*a*-5*c* illustrate temperature residuals obtained for the advectively disturbed thermal regimes shown in Figures 3*b*, 3*c*, and 3*g*, respectively. Temperature gradient ratios are calculated by normalizing vertical temperature gradients computed for each element in the mesh with respect to vertical temperature gradients calculated in the corresponding conduction-dominated case. Figures 5*d*-5*f* illustrate temperature gradient ratios calculated for the thermal regimes of Figures 3*b*, 3*c*, and 3*g*.

The plots of temperature gradient ratios indicate the possible magnitude of errors in heat flow estimates caused only by advective heat transfer. Note that additional errors may be caused by temporal variation in surface temperature and spatial variation in surface topography and thermal conductivity. Shaded regions indicate where estimates of uncorrected heat flow might be made with an error of less than 25%.

Inferences based on one-dimensional analyses of fluid flow and heat transfer suggest that the maximum advective disturbance occurs in regions of maximum fluid flux. Because temperature residuals and temperature gradient ratios reflect the disturbance of subsurface temperatures by advective heat transfer, maximum values of each might be expected in regions of maximum fluid flux. This is not the case in the two-dimensional domains presented here. For example, the absolute value of the temperature residual is greatest in a region of cooling located beneath the mountain summit (Figures 5*a*, 5*b*, and 5*c*) where rates of fluid flux within the upper permeable unit approach a minimum (indicated by widely spaced flow lines in Figures 3*b*, 3*c*, and 3*g*). Temperature gradient ratios in this region, however, differ only slightly from a value of 1.0. Therefore, although a

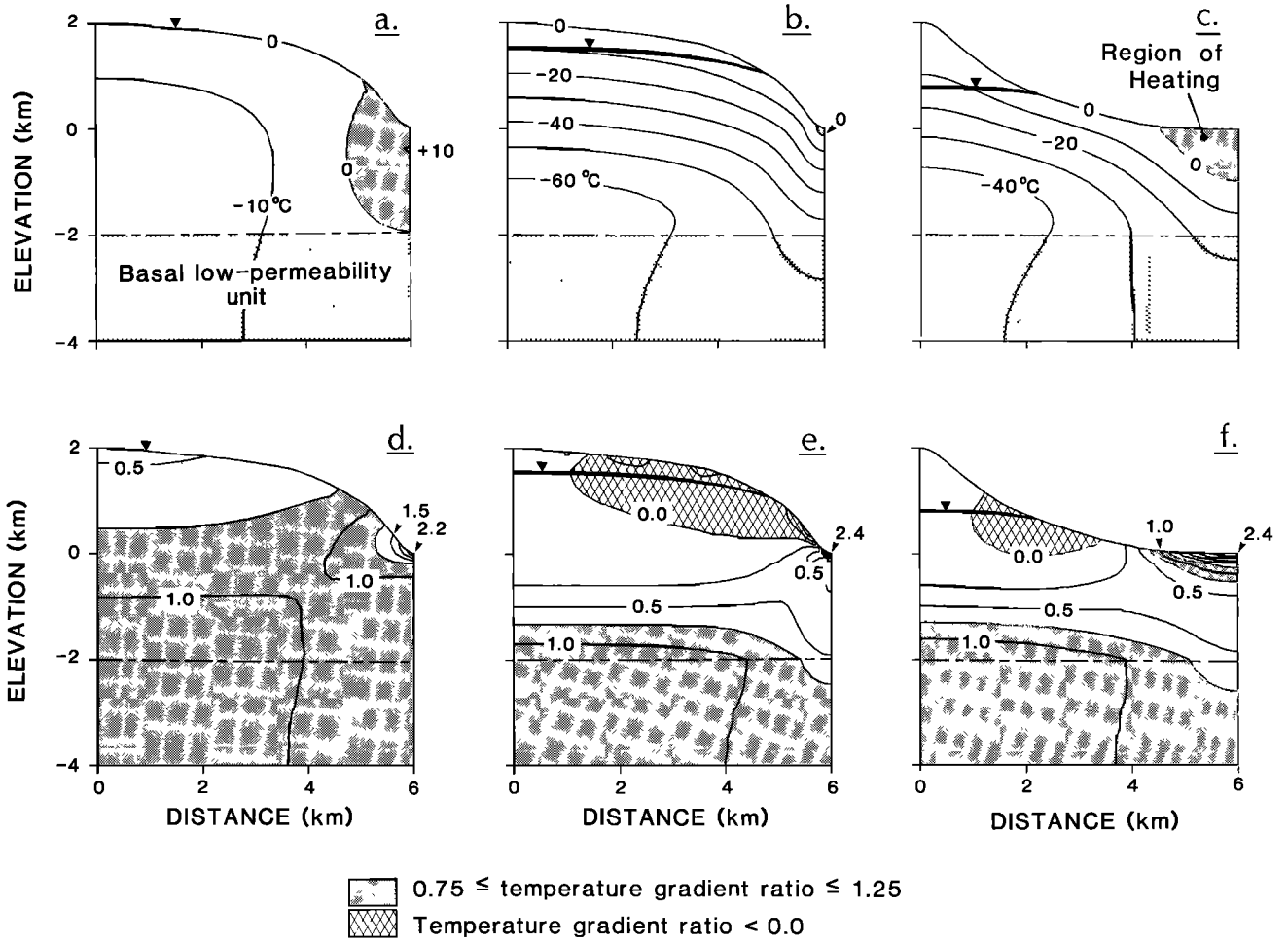

Fig. 5. Contour plots of temperature residual (°C) for convex and concave topography: (*a*) $k_u = 10^{-16}$ m^2, (*b*) $k_u = 10^{-15}$ m^2, (*c*) $k_u = 10^{-15}$ m^2 and of temperature gradient ratio, (*d*) $k_u = 10^{-16}$ m^2, (*e*) $k_u = 10^{-15}$ m^2, (*f*) $k_u = 10^{-15}$ m^2.

significant disturbance is indicated by the temperature residual, temperature gradients are relatively unaffected. In contrast, maximum values of temperature gradient ratio located in a region of maximum fluid flux near the valley floor indicate a significant disturbance, while the absolute value of temperature residual provides only limited insight into the magnitude of the advective disturbance. These results suggest that advective thermal disturbance in mountainous terrain is best assessed using a method that incorporates the two-dimensional character of the nonuniform flow systems in an explicit manner and permits both temperature residuals and temperature gradient ratios to be calculated.

Figures 5*a* and 5*b* illustrate the greater cooling that occurs when k_u is increased tenfold from 10^{-16} m^2 to 10^{-15} m^2. Increased groundwater flux absorbs thermal energy supplied at the basal boundary with less heating of the domain. As a consequence, the higher-permeability domain contains a smaller region of heating with reduced values of temperature residual. As k_u is decreased below 10^{-16} m^2, advective heat transfer is reduced, a greater percentage of the basal heat flux is transmitted by conduction, and a larger region of heating develops.

Comparing temperature residuals in Figure 5*b* with those of Figure 5*c* highlights the greater cooling that occurs in the domain with convex slope profile. Although fluid flux is similar in both convex and concave domains (the same I_z is applied at the free surface), the longer free-surface segment of the convex domain yields a total flow of groundwater about twice that of the concave domain. This provides a greater volume of fluid to absorb the basal heat flux, leads to greater cooling throughout the convex domain, and produces a smaller region of heating (Figure 5*b*).

Plots of temperature gradient ratio provide the greatest insight into the possible influence of advective disturbance on heat flow studies in mountainous terrain. For example, the maximum temperature gradient ratio exceeds 2.0 at the valley floor in each case shown in Figure 5. Additional simulations (not shown) indicate maximum temperature gradient ratios as high as 3.6 in the doubled heat flow case ($H_b = 120$ mW m^{-2}) when k_u equals 10^{-15} m^2 (Figure 3*e*). These results suggest that hydrologic effects alone could cause values of regional heat flow to be overestimated by at least 200% where thermal data are collected from boreholes located at the valley floor in terrain with permeability in excess of 10^{-17} m^2. A permeability of 10^{-17} m^2 is typical of slightly fractured crystalline or argillaceous rocks [*Freeze and Cherry*, 1979]. Therefore greater values of permeability might reasonably be expected to cause a significant advective disturbance in fractured rocks located at lower elevations on a mountain flank.

When interpreting heat flow data, it is often assumed that a

linear relationship between temperature and depth indicates the absence of a hydrologic disturbance. In low-relief terrain with relatively simple patterns of groundwater flow this is likely a reasonable assumption. Using the linearity of temperature-depth profiles to test for the presence of an advective disturbance in high-relief terrain may be misleading for two reasons. First, vertical variation in the spacing of isotherms shown in Figures 3*a*, 3*d*, and 3*f* confirms that nonlinear temperature-depth profiles should be expected in conductive thermal regimes in mountainous terrain. Thus a nonlinear temperature-depth profile does not necessarily indicate the presence of an advective disturbance. Second, temperature-depth profiles may be obtained in regions where temperature gradients appear conductive, despite a significant advective disturbance. For example, regions with near-vertical contours of temperature gradient ratio (Figures 5*d*, 5*e*, and 5*f*) indicate where perturbed temperature gradients would differ from those of the corresponding unperturbed conductive cases only by a constant multiple (the value of the gradient ratio). Analysis of temperature-depth profiles obtained in these regions would incorrectly suggest a conductive thermal regime unperturbed by groundwater flow. The likelihood for confusion is reduced in higher-permeability mountain massifs (Figures 5*e* and 5*f*) where fewer regions with near-vertical contours of temperature gradient ratio may be found.

Crosshatched areas shown in Figures 5*e* and 5*f* indicate where temperature inversions can be expected in temperature-depth borehole logs (temperature gradient ratios are less than 0.0). Such conditions are predicted to occur only when k_u exceeds 10^{-15} m^2. Isotherms found within the shaded regions of Figures 3*c*, 3*e*, and 3*g* illustrate the temperature inversions that might be expected in terrain with relief of 2 km over 6 km. Based on these modeling results, significant temperature inversions observed in boreholes located on the flank of Mount Hood, Oregon [*Steele and Blackwell*, 1982], suggest that the bulk permeability of the volcanic pile likely exceeds 10^{-15} m^2. This inferred value is within the estimated range of permeability for fractured igneous rock of 10^{-16} to 10^{-11} m^2 [*Freeze and Cherry*, 1979].

Influence of Mountain Topography

The high topographic relief of mountainous terrain amplifies the influence of surface topography on patterns of groundwater flow and the resulting advective thermal disturbance. For example, asymmetry in surface topography can cause a strong warping of isotherms near the valley floor (Figure 6) that might be mistaken for the thermal signature of a free-convection cell or a permeable fracture zone. Figure 6 represents a mountain valley with a convex slope profile on the left and a linear slope profile on the right. Mirror symmetry is assumed at vertical boundaries located at opposing summits of equal elevation. The strongly disturbed thermal regime shown in Figure 6 is obtained by assigning the reference conditions given in Table 1.

The pronounced warping of isotherms shown in Figure 6 is centered on the groundwater flow divide located within a region of closely spaced subvertical heat lines. The position of the divide reflects a balance between the total flow of groundwater beneath each slope profile. In the symmetric cases shown in Figure 3, the divide is vertical and located at the valley floor. In the asymmetric case of Figure 6, total flow through the linear slope profile is about 60% of that of

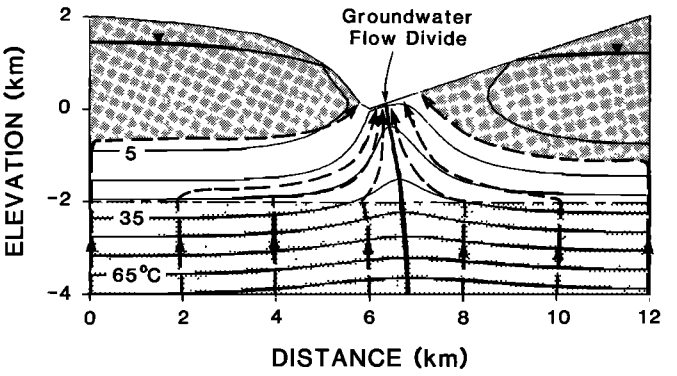

Fig. 6. Thermal regime near an asymmetric mountain valley with opposing summits of equal relief, modeled with the reference conditions of Table 1.

the convex profile. This imbalance in flow causes both the groundwater divide and the region of upwarped isotherms to be displaced to the right. The region of upwarped isotherms is displaced further to the right as the relief of the linear slope is reduced.

Figure 6 indicates that the groundwater flow divide may intersect the bedrock surface upslope of the valley floor in regions of asymmetric surface topography. Therefore chemical or thermal signatures of a subsurface heat source located beneath the left-hand convex slope may be expressed in springs discharging upslope from the valley floor on the opposing linear slope. In addition, groundwater samples collected at the valley floor may provide little information regarding conditions beneath the linear slope profile. As permeability is reduced, the warping of isotherms becomes less pronounced. The position of the groundwater flow divide, however, is unchanged.

Free Convection in Mountainous Terrain

Conceptual models developed to explain the origin of geothermal systems and the genesis of volcanogenic ore deposits often invoke the process of free convection within a mountain massif to provide elevated temperatures at shallow depth [e.g., *Henley and Ellis*, 1983]. Although these models usually incorporate the influence of a localized heat source, it is of interest to examine the interaction between topographically driven and thermally driven fluid flow in regions with uniform heat flow.

Figure 7*a* illustrates the thermal regime and patterns of fluid flow associated with development of free-convection cells in mountainous terrain, given the geologic conditions shown in Figure 7*d*. A thin low-permeability horizon (100 m thick with permeability k_i) separates two permeable units; an upper unit with k_u equal to 10^{-15} m^2 and a lower unit with k_l equal to 5×10^{-15} m^2. Path lines shown in the right-hand panel of Figure 7a depict two free-convection cells that develop in the lower permeable unit when a basal heat flow of 120 mW m^{-2} is applied and the upper and lower permeable units are isolated by setting k_i to 10^{-19} m^2. Using the definition of *Cheng* [1978], the Rayleigh number for the lower permeable unit is computed to be approximately 170. Upwarped isotherms and convergent heat lines shown in Figure 7*a* highlight the region of upwelling fluid in the free-convection cells. Heat lines pass through the low-permeability horizon to be swept in the direction of

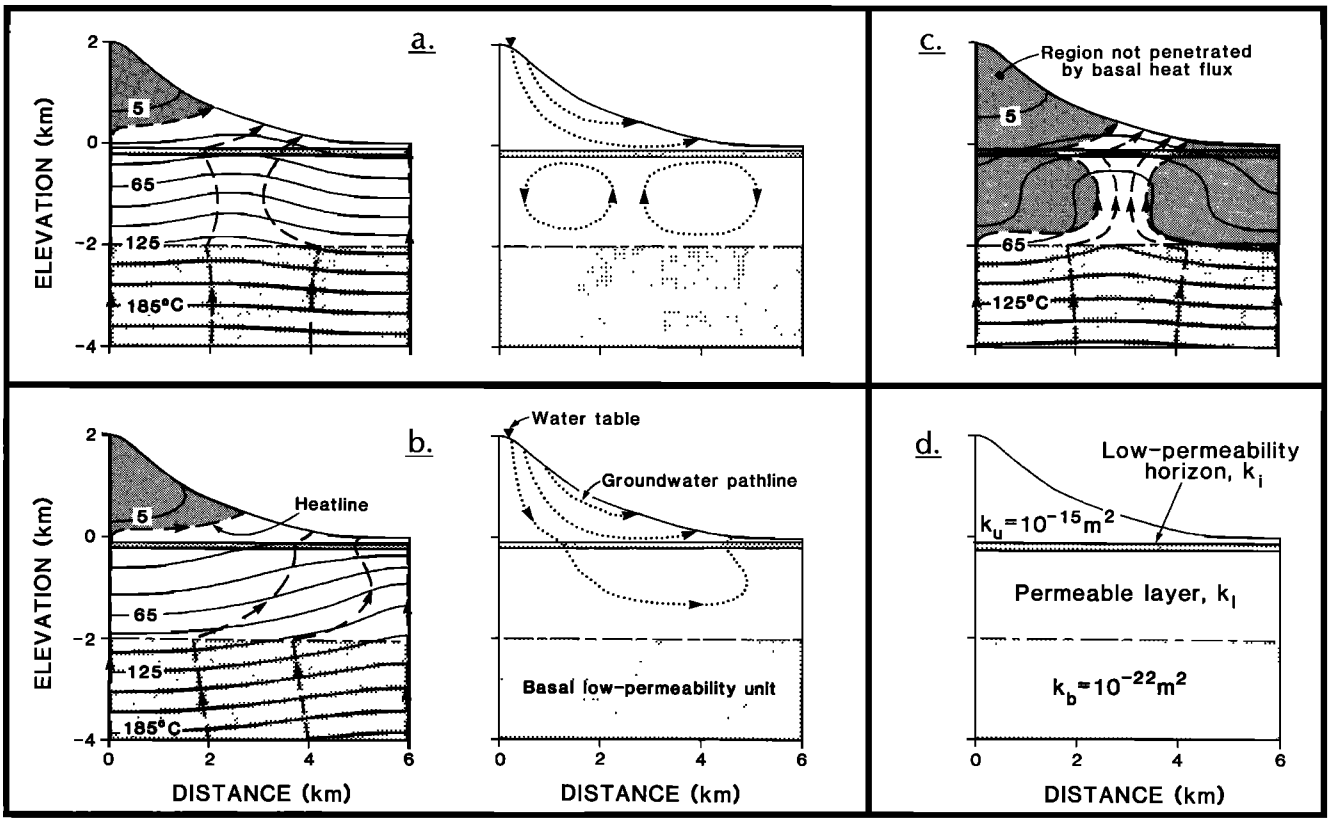

Fig. 7. Thermal regimes and patterns of groundwater flow in mixed free and forced convection scenarios with H_b = 120 mW m^{-2}, I_z = 5 x 10^{-9} m s^{-1}, and k_u = 10^{-15} m^2; (*a*) k_i = 10^{-19} m^2 and k_l = 5 x 10^{-15} m^2, (*b*) k_i = 10^{-17} m^2 and k_l = 5 x 10^{-15} m^2, (*c*) k_i = 10^{-19} m^2 and k_l = 5 x 10^{-14} m^2, (*d*) geologic conditions for simulations.

topographically driven flow in the upper permeable zone. Therefore the basal heat flux has little influence on temperatures directly beneath the mountain summit (shaded region of Figure 7*a*).

Previous studies of mixed free and forced convection specify a nonuniform heat flux at the basal boundary to represent a localized heat source that induces free convection [*Elder*, 1967; *Hanoaka*, 1980]. Modeling results shown in Figure 7, however, indicate that high-relief surface topography can cause lateral variations in the thermal regime that, in turn, cause free convection to develop in regions with uniform basal heat flux.

Increasing the permeability of the intervening unit k_i to 10^{-17} m^2 increases the groundwater flux between the upper and lower permeable units and increases the total flow through the system. Increased lateral flow in the lower permeable unit displaces the region of upwelling to the right, increases cooling beneath the mountain summit, and causes the region of warmer temperatures to migrate beneath the valley floor (Figure 7*b*). Further increasing k_i to 10^{-16} m^2 completely obliterates the free-convection cells to produce a strongly disturbed thermal regime and patterns of groundwater flow similar to those of Figure 3*f*. Under the conditions simulated here, the locations of free-convection cells and regions of elevated temperature are easily disturbed by topographically driven fluid flow because groundwater flux in the permeable upper unit (5 x 10^{-9} m s^{-1}, on average) is about 150 times greater than the buoyancy-driven fluid flux of the permeable lower unit (3 x 10^{-10} m s^{-1}, on average). Clearly, free-convection cells are less likely to be disturbed as either k_u or topographic relief are reduced, or as H_b is increased.

Increasing k_l by one order of magnitude to 5 x 10^{-14} m^2 increases the Rayleigh number to approximately 520, causes more vigorous free convection within the lower permeable layer (Figure 7c), and produces fluid flux similar in magnitude to that of the upper permeable layer (5 x 10^{-9} m s^{-1}, on average). Because there is little movement of fluid across the low-permeability horizon, the volume rate of fluid entering and exiting the domain is little changed from that found for the weakly convecting case (Figure 7*a*). The computed increase in buoyancy-driven fluid flux in the lower permeable layer, however, suggests that the free-convection cells will be better able to resist displacement by topographically driven fluid flow as the permeability of the intervening horizon is increased. In the vigorous convection case (Figure 7c), enhanced rates of buoyancy-driven fluid flow yield significant cooling throughout the lower permeable layer, except at the top of the region of upwelling, where temperatures are similar to those of the weakly convecting case (Figure 7a). Temperatures in the upper permeable unit differ little from those found in the weakly convecting case, except in the vicinity of the valley floor. These modeling results suggest that it will be difficult to define the presence of free convection within the permeable lower unit using thermal data collected in shallow boreholes.

Permeable Fracture Zones and Thermal Springs

As topographic relief increases, permeable fracture zones have a greater impact on the development of groundwater flow systems and thermal regimes [*Forster and Smith*, 1988b]. The interrelationship between permeable fracture zones and regional flow systems has received little attention, yet it has important implications for understanding the origin of fault-controlled thermal springs and assessing the effects of chemical alteration on the mechanical properties of faulted rocks. In contrast to previous model studies [*Lowell*, 1975; *Sorey*, 1978; *Kilty et al.*, 1979; *Goyal and Kassoy*, 1980; *Bodvarsson et al.*, 1982], fluid flux within the fracture zone in this study is dictated by conditions controlling the regional flow system, rather than by a specified fluid source at depth or by a specified uniform fluid flux within the fracture zone. This difference reflects the fact that our approach allows fluid to enter, or leave, the fracture zone at any point along its length. Previous workers often assume an impervious fracture wall or specify a uniform fluid flux within the fracture.

We represent fracture zones in our model with a series of line elements having uniform thickness (b) and a homogeneous equivalent porous medium permeability (k_f). Because an approximate linear relationship exists between permeability and fluid flux, various combinations of b and k_f produce the same patterns of groundwater flow in systems with matching water table configurations and matching $k_f \cdot b$ [*Forster and Smith*, 1988*b*]. The product $k_f \cdot b$ (expressed in units of $m^2 \cdot m$) is termed the transmissivity of the fracture zone and is used to characterize the simulation results. Figures 8*a* and 8*b* include a steeply dipping fracture zone, extending from the valley floor to the basal boundary. Fracture width b and permeability k_f are constant everywhere along the fracture zone. The transmissivity of the fracture zone $k_f \cdot b$ is assumed to equal $10^4 \cdot k_u$ ($m^2 \cdot m$) and might reasonably correspond to several combinations of b and k_f: b of 1 m and k_f of $10^4 \cdot k_u$, b of 10 m and k_f of $10^3 \cdot k_u$, or b of 100 m and k_f of $10^2 \cdot k_u$.

Figure 8*a* illustrates the influence of the fracture zone described above, with k_u of 10^{-15} m^2, on groundwater flow and heat transfer within the asymmetric topography of Figure 6. The effect of the permeable fracture zone is to increase the total flow of groundwater by 75%. This change in fluid flux yields a region of cooling (temperatures are depressed by at least 10°C) that is concentrated near the fault zone but extends, to a lesser degree, throughout the domain. Patterns of fluid flow and heat transfer are greatly modified because 80% of the total fluid flow, and the entire basal heat flow, is captured by the fracture zone. Furthermore, the basal heat flow is effectively masked everywhere along the upper boundary (shaded region in Figure 8*a*). Inflow from the surrounding rock mass causes fluid flux in the fracture zone to increase almost linearly, about one order of magnitude (from 10^{-6} to 10^{-5} m s^{-1}), in moving upward along the fracture zone from the top of the low-permeability unit to the bedrock surface. Rapid fluid flow in the fracture zone, fed by the surrounding rock mass, yields almost isothermal conditions along the fracture zone and a spring temperature elevated slightly above the ambient surface temperature of 10°C.

Decreasing the permeability of the surrounding rock mass to 10^{-16} m^2, while retaining the fracture transmissivity of $10^4 \cdot k_u$ ($m^2 \cdot m$), reduces fluid flux in both the fracture zone and the surrounding rock mass to yield a warmer thermal regime (Figure 8*b*) and a warmer spring temperature (24°C). The pattern of upwarped isotherms shown in Figure 8*b* differs from those of *Sorey* [1978] and *Kilty et al.* [1979], who predict large temperature gradients at shallow depths in the fracture zone and almost isothermal conditions at greater depth because they specify uniform fluid flux within the fracture zone. Reduced fluid flux at depth in the fracture zones studied here causes reduced advective heat transfer at depth and produces a more uniform temperature gradient throughout the fracture zone.

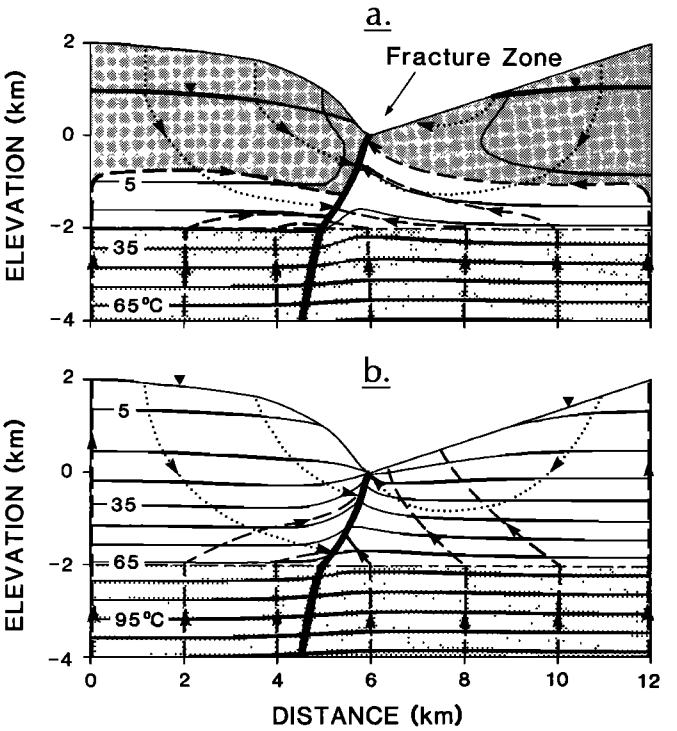

Fig. 8. Influence of a steeply dipping fracture zone with uniform $k_f \cdot b = 10^4 \cdot k_u$ ($m^2 \cdot m$) on thermal regimes within the asymmetric topography of Figure 6; (*a*) $k_u = 10^{-15}$ m^2, (*b*) $k_u = 10^{-16}$ m^2.

Patterns of fluid flow and thermal regimes shown in Figure 8 provide a quantitative framework for studying processes such as chemical alteration of faulted rocks or deposition of ore minerals in fault zones. Results presented in Figure 8 show how the permeability of the fault zone may influence the development of regional-scale groundwater flow systems and thermal regimes. The regional system must, in turn, have a strong impact on the detailed character of fluid flow and temperature within the fault zone that controls the processes of chemical alteration and mineral deposition. Our results provide support for the growing opinion that local-scale processes are best examined in the context of the regional hydrogeologic system.

Figure 9 illustrates the variation of spring temperature as a function of upper unit permeability (k_u) for both the reference and doubled heat flow cases. Maxima in spring temperature are found when rock mass permeability equals about 10^{-16} m^2. Recall that this value of k_u also produces maximum advective heating in the unfractured convex slope profile (compare temperature residuals shown in Figures 5*a* and 5*b*), reflecting the way that the overall character of the thermal regime is

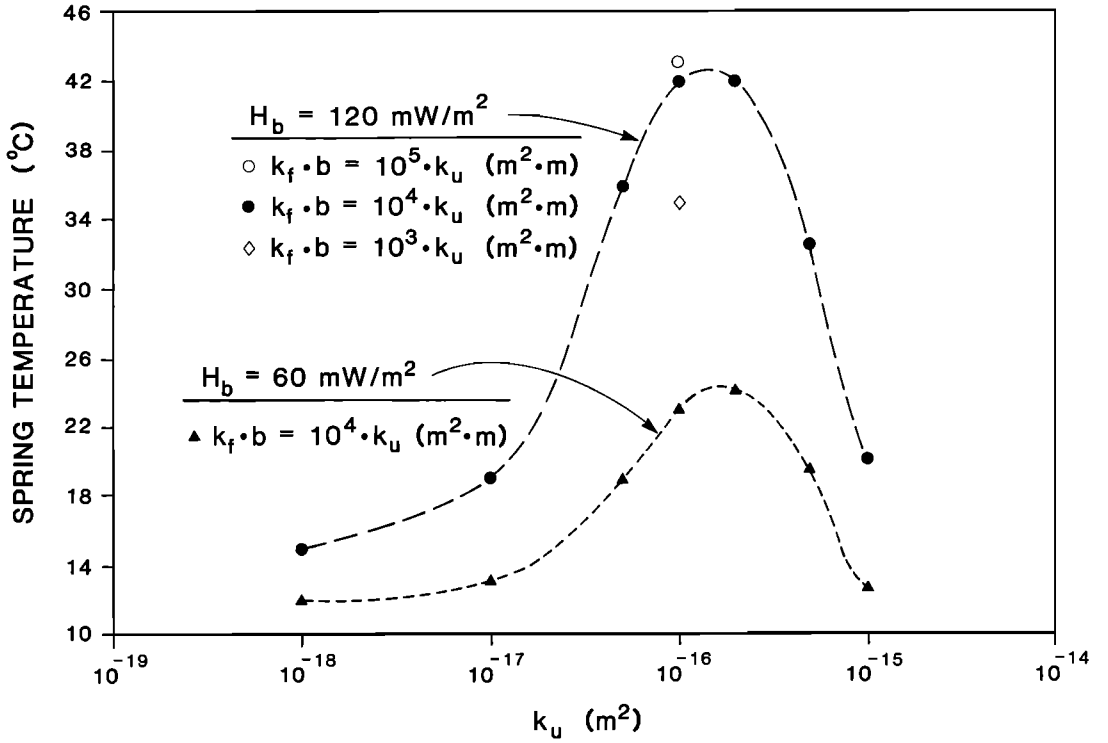

Fig. 9. Spring temperature as a function of upper zone permeability k_u, transmissivity of the fracture zone $k_f \cdot b$, and basal heat flow H_b.

controlled by regional groundwater flow through the rock mass. On a more local scale, the fracture zone provides a conduit for more rapid fluid flow that serves to concentrate the region of warming shown in Figure 5*a* within a smaller area and to produce a warmer regime near the valley floor (Figure 8*b*). Increasing k_u above 10^{-16} m^2 causes reduced spring temperatures because the larger volumetric flux of groundwater absorbs all thermal energy applied at the base of the system with little increase in temperature. Decreasing k_u below 10^{-16} m^2 causes reduced spring temperatures because fluid flow to the fracture is reduced and a greater portion of the basal heat flow is transferred by conduction through the surrounding rock mass.

The obvious dependence of spring temperature on the bulk permeability of the rock mass suggests that misleading results may be obtained when using spring temperatures to estimate the depth of groundwater circulation in a domain with a specified geothermal gradient. Changing the effective length of the fracture zone (for example, by intersecting other permeable fracture zones) modifies its influence on the thermal regime. For example, adding a second fracture zone that extends from the upland recharge area to intersect the first fracture zone at a depth of 2 km causes a greater portion of infiltrating groundwater and a greater percentage of the basal heat flow to be transmitted through the first fracture zone. The resulting increase in fluid flux and advective heat transfer through the fracture zone causes warmer spring temperature and a cooler recharge area. Conversely, reducing the length of the fracture zone to 1 km causes only a slight reduction in spring temperature because eliminating inflow to deeper regions of the fracture zone has little effect on the nonuniform pattern of fluid flux in the fracture zone.

The contrast between the transmissivity of the fracture zone $k_f \cdot b$ and the permeability of the upper unit k_u dictates the degree of thermal disturbance. In the system shown in Figure 8*b*, the fracture zone exerts its maximum influence when $k_f \cdot b$ equals about $10^4 \cdot k_u$ (m^2·m). At values of $k_f \cdot b$ in excess of $10^4 \cdot k_u$ (m^2·m), fluid flux to the fracture zone is dictated by the permeability of the surrounding rock mass and not by the transmissivity of the fracture zone. Thus, increasing $k_f \cdot b$ to $10^5 \cdot k_u$ (m^2·m) has little additional effect on the regional flow system and causes only a 1°C increase in spring temperature (open circle plotted in Figure 9). At values of $k_f \cdot b$ less than $10^4 \cdot k_u$ (m^2·m), fluid flux to the fracture zone is dictated by the transmissivity of the fracture zone ($k_f \cdot b$). As a consequence, changing the transmissivity of the fracture zone influences the rates and patterns of groundwater flow throughout the domain and has an important impact on spring temperature. For example, reducing $k_f \cdot b$ to $10^3 \cdot k_u$ (m^2·m) causes a decrease in spring temperature of 7°C (Figure 9).

Results shown in Figure 9 are representative only of the idealized geometries and conditions tested. Spring temperatures are controlled by a number of factors that are difficult to map and quantify, including fracture position, orientation, transmissivity, length, and intersection with other fractures. In addition, the three-dimensional nature of intersecting fracture zones and rugged mountainous terrain makes detailed extrapolation from two-dimensional simulations difficult. Results shown in Figure 9 suggest, however, that there is a permeability "window" wherein elevated spring temperatures are most probable ($k_u = 10^{-17}$ m^2 to 10^{-15} m^2). It should be noted that localized shallow heat sources, not considered in this study, could promote the development of high-temperature springs even when k_u lies outside this range of values.

Insight gained from our modeling results enables us to use

hot spring data to infer regional-scale permeability within the Coast Mountains of British Columbia. *Souther* [1975] notes that high-temperature phenomena such as boiling springs, fumaroles, and mud pots are absent in the Coast Mountains of British Columbia, despite elevated heat flow [*Lewis et al.*, 1985]. Sixteen thermal springs, with temperatures seldom in excess of 65°C, are scattered throughout a region of 1.3×10^4 km^2 [*Souther and Halstead*, 1973; *Souther*, 1975]. Because these springs invariably issue from fractures in crystalline rock, the associated thermal regimes are presumed to be strongly controlled by permeable fracture zones. The sparse distribution of thermal springs suggests that conditions favoring elevated spring temperatures are found only in a few localized regions. In the absence of local heat sources, the location of the observed thermal springs might indicate localized regions where bulk permeability approaches 10^{-16} m^2. Elsewhere, bulk permeability likely falls outside the range of k_u (10^{-17} m^2 to 10^{-15} m^2) required for elevated temperatures. Because crystalline terrain of the Coast Mountains is highly fractured only in localized regions, bulk permeability is likely less than 10^{-17} m^2 rather than in excess of 10^{-15} m^2.

CONCLUSIONS

1. A modeling technique that incorporates a free-surface approach within the solution for coupled fluid flow and heat transfer is developed to examine the influence of geology, surface topography, climate, and regional heat flow on the pattern and magnitude of advective disturbances of the thermal regime within a mountain massif.

2. When the water table is located beneath the bedrock surface, groundwater recharge, rather than permeability, is the appropriate factor to characterize the potential for an advective disturbance within a mountain massif.

3. Although simple geologic conditions have been modeled here, the nonuniform patterns of fluid flux and heat transfer that are observed differ markedly from the idealized patterns specified in commonly used analytical solutions [e.g., *Bredehoeft and Papadopulos*, 1965; *Domenico and Palciauskas*, 1973; *Lachenbruch and Sass*, 1977; *Mansure and Reiter*, 1979; *Ziagos and Blackwell*, 1981]. These latter solutions are more applicable when studying the small-amplitude, long-wavelength thermal disturbances associated with regional-scale groundwater flow in sedimentary basins. Thermal disturbances in mountainous terrain, however, are best assessed using methods that incorporate the two-dimensional character of the flow system in an explicit manner.

4. High-relief surface topography can cause lateral variations in the thermal regime that, in turn, promote thermally driven free-convection cells within a mountain massif subject to uniform basal heating. In the cases considered here, the thermally driven system must be isolated from the overlying topographically driven flow system by a low-permeability horizon. Otherwise, the free-convection cells will be displaced or obliterated by the topographically driven flow system.

5. Thermal springs discharging from a permeable fracture zone must be examined in the context of the regional hydrologic setting. Discharge temperatures reflect a complex interaction between fluid flow within the mountain massif and fluid flow through the fracture zone. There is a permeability "window" for the mountain massif where the temperature of a thermal spring reaches a peak value. Simple calculations relating the geothermal gradient, depth of maximum circulation, and discharge temperature do not reflect the proper physics of the process.

Acknowledgments. This work was funded by grants from the Natural Science and Engineering Research Council of Canada (NSERC) and a Graduate Research in Engineering and Technology (GREAT) award provided by the British Columbia Science Council (in cooperation with Nevin Sadlier-Brown Goodbrand Company Ltd.). Numerous discussions with David Chapman are gratefully acknowledged. Computations were carried out on an FPS 164/MAX array processor supported by an NSERC major installation grant to the University of British Columbia.

REFERENCES

Barry, R.G., *Mountain Weather and Climate*, Methuen, London, 1981.

Black, G.L., D.D. Blackwell, and J.L. Steele, Heat flow in the Oregon Cascades, in *Geology and Geothermal Resources of the Central Oregon Cascades Range, Spec. Pap. 15*, edited by G.R. Priest and B.F. Vogt, pp. 69-76, Oregon Department of Geology and Mineral Industries, Portland, 1983.

Bodvarsson, G.S., S.M. Benson, and P.A. Witherspoon, Theory of the development of geothermal systems charged by vertical faults, *J. Geophys. Res., 87*, 9317-9328, 1982.

Bredehoeft, J.D., and J.S. Papadopulos, Rates of vertical groundwater movement estimated from the Earth's thermal profile, *Water Resour. Res., 1*(2), 325-328, 1965.

Brott, C.A., D.D. Blackwell, and J.P. Ziagos, Thermal and tectonic implications of heat flow in the Eastern Snake River Plain, Idaho, *J. Geophys. Res., 86*, 11709-11734, 1981.

Cheng, P., Heat transfer in geothermal systems, *Adv. Heat Transfer, 14*, 1-105, 1978.

Domenico, P.A., and V.V. Palciauskas, Theoretical analysis of forced convective heat transfer in regional groundwater flow, *Geol. Soc. Am. Bull, 84*, 3803-3814, 1973.

Elder, J.W., Steady free convection in a porous medium heated from below, *J. Fluid Mech., 27*, 29-48, 1967.

Forster, C.B., and L. Smith, Groundwater flow systems in mountainous terrain, 1, Numerical modeling technique, *Water Resour. Res., 24*(7), 999-1010, 1988*a*.

Forster, C.B., and L. Smith, Groundwater flow systems in mountainous terrain, 2, Controlling factors, *Water Resour. Res., 24*(7), 1011-1023, 1988*b*.

Freeze, R.A., and J.A. Cherry, *Groundwater*, Prentice-Hall, Englewood Cliffs, N.J., 1979.

Freeze, R.A., and P.A. Witherspoon, Theoretical analysis of regional groundwater flow, 2, Effect of water-table configuration and subsurface permeability variation, *Water Resour. Res., 3*, 623-624, 1967.

Garven, G., and R.A. Freeze, Theoretical analysis of the role of groundwater flow in the genesis of stratabound ore deposits, 2, Quantitative results, *Am. J. Sci., 284*, 1125-1174, 1984.

Gosnold, W.D., Heat flow and ground water flow in the great plains of the United States, *J. Geody., 4*, 247-264, 1985.

Goyal, K.P., and D.R. Kassoy, Fault zone controlled charging of a liquid-dominated geothermal reservoir, *J. Geophys. Res., 85*, 1867-1875, 1980.

Hanoaka, N., Numerical model experiment of hydrothermal system-Topographic effects, *Bull. Geol. Surv. Jpn., 31*(7), 321-332, 1980.

Henley, R.W., and A.J. Ellis, Geothermal systems ancient and modern: A geochemical review, *Earth Sci. Rev., 19*, 1-50, 1983.

Ingebritsen, S.E., and M.L. Sorey, A quantitative analysis of the Lassen hydrothermal system, north central California, *Water Resour. Res., 21*(6), 853-868, 1985.

Kilty, K., D.S. Chapman, and C.W. Mase, Forced convective heat transfer in the Monroe Hot Springs geothermal area, *J. Volcanol. Geotherm. Res., 6*, 257-272, 1979.

Kimura, S., and A. Bejan, The "heatline" visualization of convective heat transfer, *J. Heat Transfer, 105*, 917-919, 1983.

Lachenbruch, A.H., and J.H. Sass, Heat flow in the United States and the thermal regime of the crust, in *The Earth's Crust, Geophys. Monogr. Ser.*, vol. 20, edited by J.G. Heacock, pp. 626-675, AGU, Washington, D. C., 1977.

Lewis, T.J., A.M. Jessop, and A.S. Judge, Heat flux measurements in southwestern British Columbia: The thermal consequences of plate tectonics, *Can. J. Earth Sci., 22*, 1262-1273, 1985.

Lowell, R.P., Circulation in fractures, hot springs, and convective heat transport on mid-ocean ridge crests, *Geophys. J. R. Astron. Soc., 40*, 351-365, 1975.

Majorowicz, J.A., F.W. Jones, H.L. Lam, and A.M. Jessop, Terrestrial heat flow and geothermal gradients in relation to hydrodynamics in the Alberta Basin, Canada, *J. Geody., 4*, 265-283, 1985.

Mansure, A.J., and M. Reiter, A vertical groundwater movement correction for heat flow, *J.Geophys. Res., 84*, 3490-3496, 1979.

Mase, C.W., J.H. Sass, A.H. Lachenbruch, and J.R. Munroe, Preliminary heat-flow investigations of the California Cascades, *U.S. Geol. Surv. Open File Rep. 82-150*, 1982.

Neuzil, C.E., Groundwater flow in low-permeability environments, *Water Resour. Res., 22*(8), 1163-1196, 1986.

Reader, J.F., and B.D. Fairbank, Heat flow in the vicinity of the Meager Volcanic Complex, southwestern British Columbia, *Trans. Geotherm. Resour. Counc., 7*, 535-539, 1983.

Ross, B., A conceptual model of deep unsaturated zones with negligible recharge, *Water Resour. Res., 20*(11), 1627-1629, 1984.

Smith, L., and D.S. Chapman, On the thermal effects of groundwater flow, 1, Regional scale systems, *J. Geophys. Res., 88*, 593-608, 1983.

Smith, L., and D.S. Chapman, The influence of water table configuration on the near-surface thermal regime, *J. Geody., 4*, 183-198, 1985.

Sorey, M.L., Numerical modeling of liquid geothermal systems, *U.S. Geol. Surv. Prof. Pap. 1044-D*, 1978.

Souther, J.G., Geothermal potential of western Canada, in *Proceedings of 2nd U.N. Symposium on Development and Use of Geothermal Resources*, vol. 1, pp. 259-267, United Nations, New York, 1975.

Souther, J.G. and E.C. Halstead, Mineral and thermal waters of Canada, *Can. Dep. Energy Mines Resour., Pap. 73-18*, 1973.

Steele, J.L., and D.D. Blackwell, Heat flow in the vicinity of the Mount Hood Volcano, Oregon, in *Geology and Geothermal Resources of the Mount Hood Area, Oregon, Spec. Pap. 14*, Geology and Mineral Industries, pp. 31-42, Portland, 1982.

Thompson, W.T., How and why to distinguish between mountains and hills, *Prof. Geog., 16*, 6-8, 1964.

Willet, S.D., and D.S. Chapman, On the use of thermal data to resolve and delineate hydrologic flow systems in sedimentary basins: An example from the Uinta Basin, Utah, in *Proceedings of the Third Annual Canadian/American Conference on Hydrology, Hydrogeology of Sedimentary Basins: Application to Exploration and Exploitation*, edited by B. Hitchon, S. Bachu, and C. Sauveplane, Dublin, Ohio, 159-168, 1987.

Woodbury, A.D., and L. Smith, On the thermal effects of three-dimensional groundwater flow, *J. Geophys. Res., 90*, 759-767, 1985.

Woodbury, A.D., and L. Smith, Simultaneous inversion of hydrogeologic and thermal data, 2, Incorporation of thermal data, *Water Resour. Res., 24*(3), 356-372, 1988.

Ziagos, J.P., and D.D. Blackwell, A model for the effect of horizontal fluid flow in a thin aquifer on temperature-depth profiles, *Trans. Geotherm. Resour. Counc., 5*, 221-223, 1981.

C. Forster, Department of Geology, Utah State University, Logan, UT 84322.

L. Smith, Department of Geological Sciences, University of British Columbia, Vancouver, British Columbia Canada V6T 2B4.

(Received August 14, 1987;
revised January 31, 1989;
accepted November 29, 1988)